CellPress
Partner Journal

Molecular Plant
Research article

The long non-coding RNA *PILNCR2* increases low phosphate tolerance in maize by interfering with miRNA399-guided cleavage of *ZmPHT1*s

Yafei Wang[1,3], Zhonghua Wang[2,3], Qingguo Du[1], Kai Wang[1], Chunqin Zou[2] and Wen-Xue Li[1,*]

[1]National Engineering Laboratory for Crop Molecular Breeding, Institute of Crop Sciences, Chinese Academy of Agricultural Sciences, Beijing 100081, China

[2]College of Resources and Environmental Sciences, National Academy of Agriculture Green Development, Key Laboratory of Plant-Soil Interactions, Ministry of Education, China Agricultural University, Beijing 100193, China

[3]These authors contributed equally to this article.

***Correspondence: Wen-Xue Li (liwenxue@caas.cn)**

https://doi.org/10.1016/j.molp.2023.05.009

ABSTRACT

The open reading regions of *ZmPHT1*s (inorganic phosphate [Pi] transporters) in maize possess target sites of microRNA399 (miR399). However, the relationship between miR399 and *ZmPHT1*s and its functional importance in response to Pi deficiency remain to be explored. We show here that *ZmPHT1*;*1*, *ZmPHT1*;*3*, and *ZmPHT1*;*13* are the targets of ZmmiRNA399. We found that a long non-coding RNA, *PILNCR2* (Pi-deficiency-induced lncRNA 2), is transcribed from the opposing DNA strand of *ZmPHT1*;*1* and predominantly localized in the cytoplasm. A ribonuclease protection assay and an RNA–RNA binding assay showed that *PILNCR2* and *ZmPHT1*s could form the RNA/RNA duplexes *in vivo* and *in vitro*. A co-expression assay in *N. benthamiana* revealed that the *PILNCR2*/*ZmPHT1* RNA/RNA duplexes interfere with miR399-guided cleavage of *ZmPHT1* mRNAs. Overexpression of *PILNCR2* increased low-Pi tolerance in maize, whereas its knockout and knockdown decreased low-Pi tolerance in maize. Consistently, *ZmPHT1;3* and *ZmPHT1;13* mRNA abundance was increased in transgenic plants overexpressing *PILNCR2* but reduced in its knock-out mutants, suggesting that *PILNCR2* positively regulates the mRNA abundance of *ZmPHT1*;*3* and *ZmPHT1*;*13* in maize. Collectively, these results indicate that *PILNCR2* plays an important role in maize Pi homeostasis by interfering with miRNA399-guided cleavage of *ZmPHT1* mRNAs.

Key words: long non-coding RNA, miRNA, RNA/RNA duplex, post-transcriptional regulation, maize

Wang Y., Wang Z., Du Q., Wang K., Zou C., and Li W.-X. (2023). The long non-coding RNA *PILNCR2* increases low phosphate tolerance in maize by interfering with miRNA399-guided cleavage of *ZmPHT1*s. Mol. Plant. **16**, 1146–1159.

INTRODUCTION

Phosphorus (P) is an essential nutrient for plant growth and development. Plants mainly acquire P in the form of inorganic phosphate (Pi). Pi can easily be fixed by aluminum and iron in acidic soils and by calcium in alkaline soils, which limits its diffusion in soil and therefore its availability to plants (Péret et al., 2011). Because of the slow diffusion of Pi in soil, ~70% of global arable land is estimated to be deficient in Pi (Lopez-Arredondo et al., 2014). Pi deficiency has become a key environmental constraint to crop productivity worldwide (Lopez-Arredondo et al., 2014; Lambers, 2022).

Changes in gene expression play an important role in plant responses to Pi deficiency. Transcriptomic analyses of multiple plant species have shown that Pi starvation affects the mRNA abundance of more than 20% of the genes in the plant transcriptome (Paz-Ares et al., 2022). Transcription factors have been found to regulate Pi starvation responses by controlling the expression of downstream genes. Among the diverse Pi-responsive transcription factors, *SENSITIVE TO PROTON RHIZOTOXICITY 1* and *PHOSPHATE STARVATION RESPONSES* have been identified as the central regulators in local and systemic signaling, respectively (Ried et al., 2021; Tian et al., 2021; Das et al., 2022; Guo et al., 2022; Paz-Ares et al., 2022). With the discovery of non-coding RNAs (ncRNAs), research has increasingly indicated their importance in transcriptional, post-transcriptional, or translational gene regulation.

Published by the Molecular Plant Shanghai Editorial Office in association with Cell Press, an imprint of Elsevier Inc., on behalf of CSPB and CEMPS, CAS.

ncRNAs include mainly microRNAs (miRNAs), small interfering RNAs, and long ncRNAs (lncRNAs). miRNAs are processed from *MIRNA* genes with a highly self-complementary structure by the ribonuclease III-like enzyme Dicer. The processed miRNAs are selectively loaded into AGO1 or AGO10 and form RNA-induced silencing complexes (RISCs) (Baumberger and Baulcombe, 2005; Zhu et al., 2011). miRNAs guide RISCs to target mRNAs with perfect or nearly perfect base pairing and negatively regulate the abundance of target mRNA by cleavage or translation repression in the cytoplasm (Song et al., 2019). Because RISCs cannot unfold target RNA secondary structures, cleavage by RISCs is highly dependent on target site accessibility (Ameres et al., 2007).

miRNA399 was the first miRNA reported to participate in Pi-deprivation responses in plants. By suppressing the ubiquitin-conjugating E2 enzyme PHO2, overexpression of miRNA399 led to over-accumulation of Pi in *Arabidopsis* shoots under Pi-sufficient conditions (Fujii et al., 2005; Chiou et al., 2006). The miRNA399–PHO2 module was also demonstrated to regulate uptake, translocation, and remobilization of Pi in rice (Hu et al., 2011). Previous results from our laboratory also showed that the miRNA399–PHO2 signaling pathway is conserved among plant species and that this pathway is important for modulating Pi homeostasis in maize (Du et al., 2018). The latter study also found, however, that the difference in total P concentration between transgenic maize overexpressing *MIRNA399b* and the wild type (WT) was smaller under Pi-deficient conditions than under Pi-sufficient conditions (Du et al., 2018). In addition, Pi transporters (PHTs) were predicted to be targeted by miRNA399 in maize (Zhang et al., 2009; Pei et al., 2013). If that prediction is correct, it would be inconsistent with the typical Pi-toxicity phenotypes observed in transgenic maize overexpressing *MIRNA399b*. Consequently, the miRNA399 pathway that modulates Pi homeostasis in maize requires further investigation.

lncRNAs, which are typically longer than 200 nt, have functions that are independent of their protein-coding potential (Wierzbicki et al., 2021). In mammals, lncRNAs function in diverse cellular processes, such as chromatin architecture modification (Minajigi et al., 2015), mRNA turnover (Kleaveland et al., 2018), and translation (Ingolia et al., 2011). Compared with research on lncRNAs in mammals, research on lncRNAs in plants is still at an early stage. The functions of only a few plant lncRNAs (including *XLOC_057324*, *COOLAIR*, *HIDDEN TREASURE 1*, *LAIR*, *MAS*, *SVALAK*, and *VAS*) have been characterized in detail (Swiezewski et al., 2009; Heo and Sung, 2011; Wang et al., 2014a, 2014b, 2018; Zhang et al., 2014; Kindgren et al., 2018; Zhao et al., 2018; Xu et al., 2021). The limited evidence suggests, however, that lncRNAs could be important modulators of plant development and stress adaptation. *cis-NATPHO1;2* was recently demonstrated to act as a translational enhancer for its cognate PHO1;2 and to affect Pi homeostasis in rice (Jabnoune et al., 2013). Previous results from our laboratory indicated that *PILNCR1* (Pi-deficiency-induced lncRNA 1) can inhibit ZmmiRNA399-guided cleavage of *ZmPHO2* mRNAs and that this reduction depends on complementary regions in *PILNCR1* and ZmmiRNA399 (Du et al., 2018). Together, these results suggest that lncRNAs may function in Pi homeostasis in plants.

In the present research, we show that mRNAs of *ZmPHT1;1*, *ZmPHT1;3*, and *ZmPHT1;13* can be cleaved by ZmmiRNA399. We also identify a lncRNA, *PILNCR2*, that is transcribed from the opposing DNA strand of *ZmPHT1;1*. We then demonstrate that *PILNCR2* can form an RNA/RNA duplex with *ZmPHT1*s that interferes with miRNA399-guided cleavage of *ZmPHT1* mRNAs. As a result, overexpression of *PILNCR2* increases low-Pi tolerance in maize, whereas knockdown or knockout of *PILNCR2* decreases low-Pi tolerance. Taken together, our results describe a new way in which lncRNAs affect miRNA functions in plants.

RESULTS

Expression profiling of *ZmPHT1*s in response to Pi deficiency

The PHT1 family in maize has 13 members (Liu et al., 2016). Five members (*ZmPHT1;1*, *ZmPHT1;3*, *ZmPHT1;7*, *ZmPHT1;8*, and *ZmPHT1;13*) were predicted to be potential targets of ZmmiRNA399, but this prediction has not been verified (Supplemental Table 1) (Zhang et al., 2009; Dai et al., 2018). Previous results from our laboratory clearly showed that ZmmiRNA399 is specifically upregulated by Pi deficiency (Du et al., 2018). If *ZmPHT1;1*, *ZmPHT1;3*, *ZmPHT1;7*, *ZmPHT1;8*, and *ZmPHT1;13* are the targets of ZmmiRNA399, then their mRNA abundance should be downregulated by Pi deficiency. We first checked our strand-specific RNA libraries from roots of the inbred lines CCM454 and 31778 that had been subjected to Pi stress for 2 and 8 days (Du et al., 2016). The expression levels of *ZmPHT1;1*, *ZmPHT1;3*, and *ZmPHT1;13* were significantly upregulated by Pi deficiency in both inbred lines, CCM454 and 31778 (Supplemental Figure 1A). Because of the low mRNA abundance of *ZmPHT1;7* and *ZmPHT1;8* (Supplemental Figure 1A), we did not select them for further research.

We next assessed the responses of *ZmPHT1;1*, *ZmPHT1;3*, and *ZmPHT1;13* to Pi stress using quantitative real-time RT–PCR. Consistent with our RNA sequencing data, Pi deficiency significantly induced the expression levels of *ZmPHT1;1*, *ZmPHT1;3*, and *ZmPHT1;13* (Supplemental Figure 1B). For example, after maize had been transferred to Pi-deficient medium for 12 days, *ZmPHT1;3* mRNA levels increased approximately 40-fold in roots (Supplemental Figure 1B). This is inconsistent with the possibility that increases in the expression of miRNA399 under Pi deficiency decrease *ZmPHT1* mRNA levels.

ZmPHT1;1, *ZmPHT1;3*, and *ZmPHT1;13* are the targets of ZmmiRNA399

To further characterize the possible relationships between miRNA399 and the *ZmPHT1*s, we performed transient co-expression assays in *N. benthamiana*. Both *ZmPHT1* and miRNA399 constructs were expressed under the control of the *35S* promoter. Small RNA analysis clearly showed that miRNA399 was expressed in all of the co-expression samples (Supplemental Figure 2). Transcripts of the *ZmPHT1*s were decreased significantly when these *ZmPHT1*s were co-expressed with *MIRNA399b* (Figure 1A). We also analyzed *ZmPHT1;1*, *ZmPHT1;3*, and *ZmPHT1;13* transcripts in *MIRNA399b*-overexpressing transgenic maize (Du et al., 2018). Overexpression of *MIRNA399b* clearly reduced the mRNA levels of *ZmPHT1;1*, *ZmPHT1;3*, and

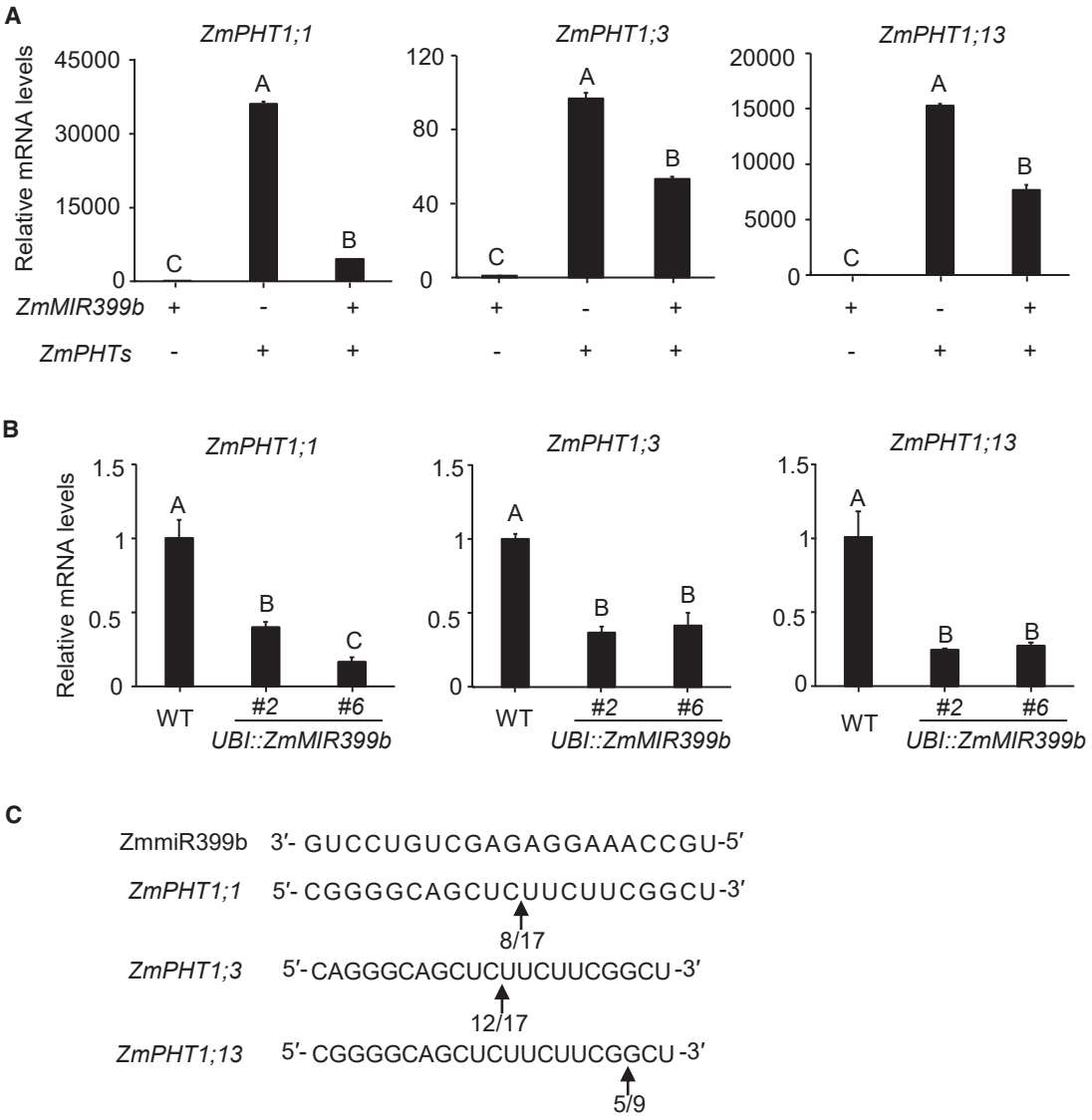

Figure 1. ZmmiRNA399 post-transcriptionally regulates the mRNA abundance of *ZmPHT1;1*, *ZmPHT1;3*, and *ZmPHT1;13*.

(A) Co-expression of *ZmMIR399b* and *ZmPHT1* expression constructs in *N. benthamiana*. Real-time RT–PCR quantifications were normalized to the expression of tobacco 18S rRNA.

(B) Detection of *ZmPHT1* transcripts in *ZmMIR399b*-overexpressing transgenic maize by real-time RT–PCR. qRT–PCR quantifications were normalized to the expression of *ZmActin1*.

Error bars in **(A)** and **(B)** represents standard errors of three biological replicates. Means with the same letter are not significantly different at $p < 0.01$ according to one-way ANOVA followed by Tukey's multiple comparison test.

(C) *ZmPHT1* mRNA cleavage sites detected by 5′-RACE. Numbers indicate the frequency of cleavage at the site.

ZmPHT1;*13* (Figure 1B). These results suggested that *ZmPHT1*;*1*, *ZmPHT1*;*3*, and *ZmPHT1*;*13* are potential targets of miRNA399 in maize.

A 5′ rapid amplification of cDNA ends (RACE) assay was also performed to map the potential cleavage sites in *ZmPHT1*;*1*, *ZmPHT1*;*3*, and *ZmPHT1*;*13* using RNA from maize seedlings that had been subjected to Pi deficiency for 6 days. The identified cleavage site in *ZmPHT1*;*1* and *ZmPHT1*;*3* was located at the position opposite nucleotides 10 and 11 of miRNA399, and that in *ZmPHT1*;*13* was located at the position opposite nucleotides 3 and 4 of miRNA399 (Figure 1C). These results further showed that miRNA-guided cleavage existed between miRNA399 and mRNAs of *ZmPHT1*;*1*, *ZmPHT1*;*3*, and *ZmPHT1*;*13*.

Characteristics of *PILNCR2*

The upregulation of miRNA399 and *ZmPHT1*;*1*, *ZmPHT1*;*3*, and *ZmPHT1*;*13* by Pi deficiency suggested the presence of another regulatory mechanism affecting miRNA399-guided repression of *ZmPHT1*s in maize. One possibility was regulation by a lncRNA. To investigate this possibility, we examined our lncRNA libraries that had previously been constructed from inbred lines CCM454 and 31778 subjected to Pi deficiency (Du et al., 2018). *PILNCR2*

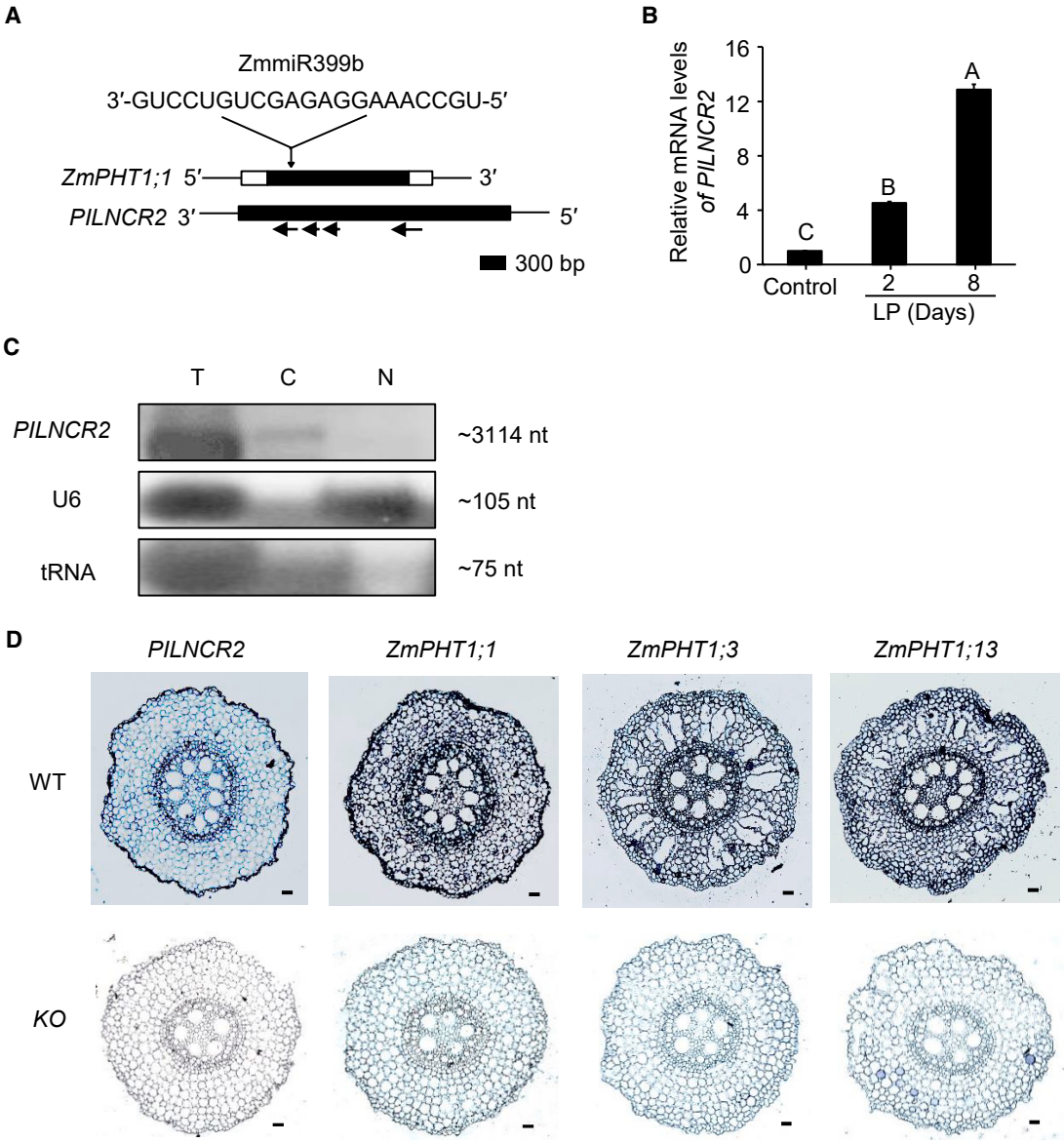

Figure 2. Expression patterns of *PILNCR2*.

(A) Diagram of the complementary region of *PILNCR2* and *ZmPHT1;1*. Black boxes indicate exons. Vertical arrow represents the target position of miRNA399. Horizontal arrows show the four potential ORFs in *PILNCR2* predicted by SnapGene.

(B) Effects of Pi deficiency on the mRNA abundance of *PILNCR2*. qRT–PCR quantifications were normalized to the expression of *ZmGAPDH*. Error bars represent standard errors of three biological replicates. Means with the same letter are not significantly different at $p < 0.01$ according to one-way ANOVA followed by Tukey's multiple comparison test.

(C) Detection of the subcellular locations of *PILNCR2* by northern blot analysis. U6 and tRNA were used as nuclear and cytosolic RNA markers, respectively.

(D) Expression patterns of *PILNCR2*, *ZmPHT1;1*, *ZmPHT1;3*, and *ZmPHT1;13* in roots of wild-type (WT) and *PILNCR2*-knockout (*KO*) transgenic maize as determined by *in situ* hybridization analysis. Scale bars: 50 μm. LP, low Pi; T, total RNA; C, cytosolic RNA; N, nuclear RNA.

attracted our attention. Unlike *PILNCR1*, which was previously found to contain a region complementary to ZmmiR399 (Du et al., 2018), *PILNCR2* was transcribed from the opposite DNA strand of *ZmPHT1;1* and was complementary to the full cDNA sequence of *ZmPHT1;1* (Figure 2A). Using 5′- and 3′-RACE PCR, we isolated a 3114-bp cDNA clone containing a 26-bp poly-A tail (Supplemental Figure 3).

We treated the extracted RNA with calf intestine alkaline phosphatase (CIP). *PILNCR2* could be detected in the CIP-treated sample by 5′-RACE PCR (Supplemental Figure 4), indicating the existence of capped-*PILNCR2* transcripts. The occurrence of both a poly-A tail at the 3′ terminus and a cap at the 5′ end suggested that transcription of *PILNCR2* was dependent on RNA polymerase II.

SnapGene (https://www.snapgene.com/snapgene-viewer/) predicted that four potential open reading frames (ORFs) were present in *PILNCR2* (Supplemental Figure 3). BLASTP analysis did not identify homologs of these potential ORFs in UniProt (https://www.uniprot.org/). The predicted ORFs were cloned,

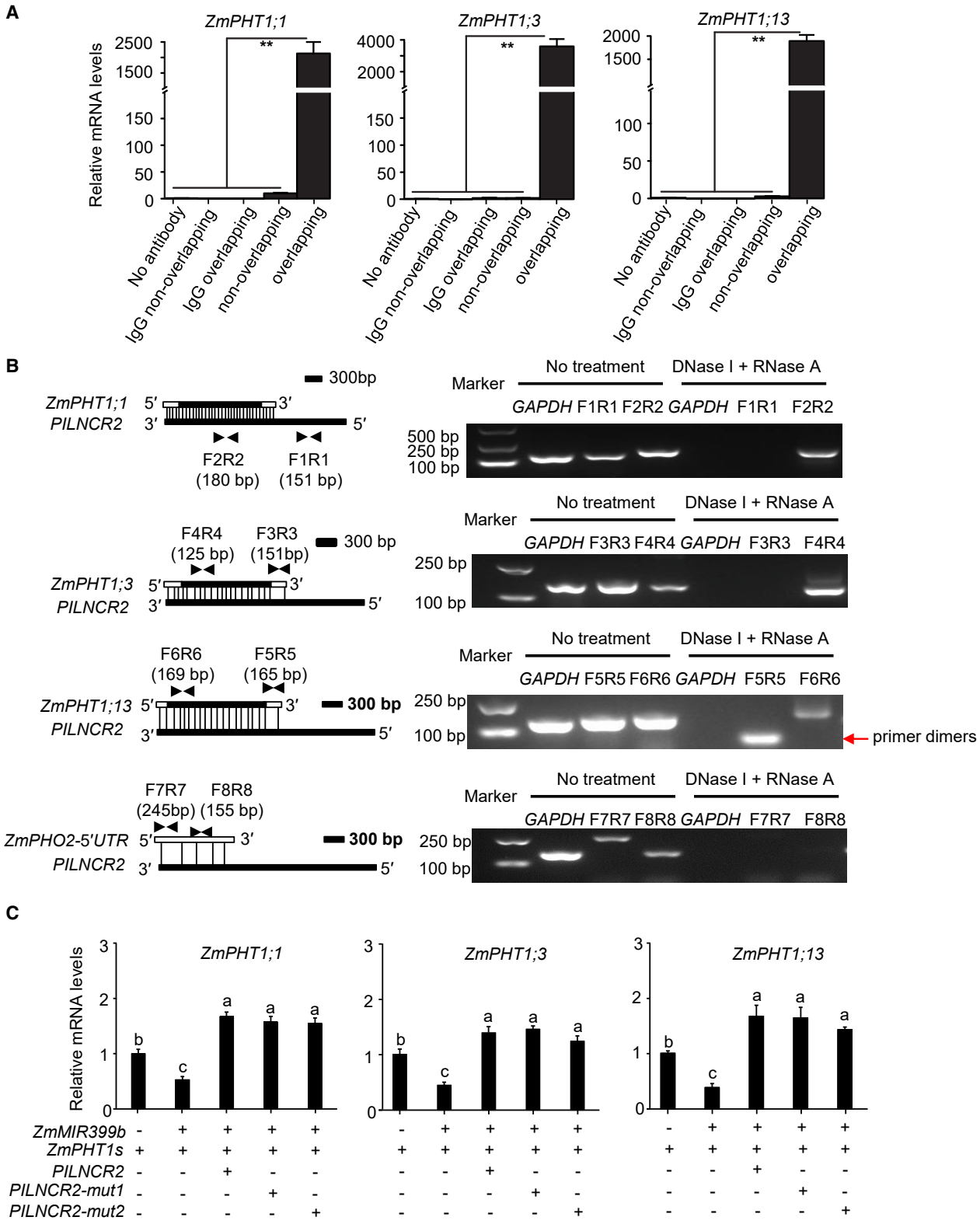

Figure 3. *PILNCR2* interacts with *ZmPHT1*s.

(A) *In vitro* RNA–RNA interaction assay of *PILNCR2* with *ZmPHT1*;*1*, *ZmPHT1*;*3*, or *ZmPHT1*;*13*. The controls included no anti-BrdU monoclonal antibody (mAb), immunoglobulin G antibody plus the *PILNCR2* region that did not overlap with *ZmPHT1*;*1*, immunoglobulin G antibody plus the *PILNCR2* region that overlapped with *ZmPHT1*;*1*, and anti-BrdU mAb plus the *PILNCR2* region that did not overlap with *ZmPHT1*;*1*. Data were normalized to the no anti-BrdU mAb treatment. Error bars represent standard errors of three biological replicates. Asterisks indicate significant differences between the anti-BrdU mAb plus *PILNCR2* region that overlapped with *ZmPHT1*;*1* treatment and the other treatments based on *t*-tests ($p < 0.01$).

(legend continued on next page)

and ORFs–GFP/GFP–ORFs were constructed and transiently expressed in maize mesophyll protoplasts. Although the plasmids were successfully transformed into maize mesophyll protoplasts, GFP signals were not detected in these protoplasts (Supplemental Figures 5 and 6). The results suggested that *PILNCR2* is a lncRNA.

Expression patterns of *PILNCR2*

Expression analysis showed that Pi deficiency upregulated the mRNA abundance of *PILNCR2* (Figure 2B). This indicated that *PHT1*s and *PILNCR2* were co-regulated by Pi deficiency. We then investigated the partitioning of *PILNCR2* between the nucleus and cytoplasm by northern blot analysis. The cytosolic location of tRNA and the nuclear location of U6 verified the purification of our fractionated nuclear and cytosolic extracts (Figure 2C). We found that *PILNCR2* was predominantly localized in the cytoplasm (Figure 2C).

To further explore the possible relationship between *PILNCR2* and *ZmPHT1*s, we examined the expression patterns of *PILNCR2*, *ZmPHT1*;*1*, *ZmPHT1*;*3*, and *ZmPHT1*;*13* by *in situ* hybridization. Because of the low abundance of *PILNCR2* and *ZmPHT1*s in maize under Pi-sufficient conditions, maize roots subjected to Pi deficiency for 8 days were sampled to assess the expression patterns of *PILNCR2* and *ZmPHT1*s. The specific fragment of *PILNCR2* that did not overlap with *ZmPHT1*s was used as a probe for *in situ* hybridization analysis of *PILNCR2*. *PILNCR2* was detected throughout the root (Figure 2D). Because *ZmPHT1*;*1* completely overlapped with *PILNCR2*, *PILNCR2*-knockout transgenic maize were used for *in situ* hybridization analysis of *ZmPHT1*s. *ZmPHT1*;*1*, *ZmPHT1*;*3*, and *ZmPHT1*;*13* were also detected throughout the root (Figure 2D).

Interactions between *PILNCR2* and *ZmPHT1*s

The chromatin location and Pi-deficiency induction of *PILNCR2* and *ZmPHT1*;*1* were reminiscent of a previously reported *NERF*/*NFYA5* gene pair (Gao et al., 2015); in this gene pair, siRNANERF (small interfering RNA RING FINGER) originating from the overlapping region (OR) was found to mask and/or compete with miRNA169, thereby impairing miRNA169-guided cleavage of *NFYA5* mRNAs. We therefore first determined whether small interfering RNAs (siRNAs) were present in the OR of *PILNCR2* and *ZmPHT1*;*1*. After alignment with libraries deposited at NCBI (SRP060481 and SRP029451), no siRNAs were detected in the OR of *PILNCR2* or *ZmPHT1*;*1*, and this result was further verified by small RNA northern blots (Supplemental Figure 7). We inferred that siRNAs are not involved in miRNA399-guided cleavage of *ZmPHT1s*.

In an *in vitro* RNA–RNA binding assay, the relative mRNA levels of *ZmPHT1*;*1*, *ZmPHT1*;*3*, and *ZmPHT1*;*13* were much higher in the treatment with anti-BrdU monoclonal antibody plus the *PILNCR2* region overlapping *ZmPHT1*;*1* than in the other treatments (Figure 3A). To directly examine the interaction between *PILNCR2* and *ZmPHT1*s *in vivo*, we performed a ribonuclease protection assay. After all genomic DNA contamination and single-stranded RNAs were removed, the residual endogenous double-stranded RNAs were used for RT–PCR. An amplification product was detected only in the OR of *PILNCR2* and *ZmPHT1*s (Figure 3B). *ZmPHO2* is a target of ZmmiR399 (Du et al., 2016). We thus chose the 5′ UTR of *ZmPHO2*, which contained six ZmmiR399 cleavage sites (Du et al., 2018), as a negative control for the ribonuclease protection assay. No amplification product was detected in the potential OR of *PILNCR2* and *ZmPHO2* (Figure 3B). These results suggested that *PILNCR2* and *ZmPHT1*s could form an RNA/RNA duplex *in vivo*.

ZmPHT1;*1*, *ZmPHT1*;*3*, or *ZmPHT1*;*13* was then co-expressed with *ZmMIR399b* and/or *PILNCR2* under the control of the *35S* promoter in *N. benthamiana*. After 2 days, RNA was extracted, and *ZmPHT1* expression was analyzed by quantitative RT–PCR. Small RNA gel blots prepared from the same samples clearly showed that *ZmMIRNA399* was highly expressed in all co-expression samples (Supplemental Figure 8). When *ZmPHT1;1, ZmPHT1;3, and ZmPHT1;13 were* co-expressed with *ZmMIRNA399b*, their mRNA levels decreased significantly (Figure 3C). Interestingly, *ZmMIRNA399b*-guided repression of *ZmPHT1*;*1*, *ZmPHT1*;*3*, and *ZmPHT1*;*13* mRNAs was not observed when they were co-expressed with *PILNCR2* (Figure 3C). We also introduced five mutations into, or deleted, the *PILNCR2* region that had a sequence similar to that of mature ZmmiR399 (*PILNCR2-mut1* and *PILNCR2-mut2*, respectively). *PILNCR2-mut*s also interfered with the *ZmMIRNA399b*-guided repression of *ZmPHT1*s (Figure 3C). These results suggested that *PILNCR2-mut*s did not affect the formation of *PILNCR2/ZmPHT1* duplexes and that the duplexes interfered with miRNA399-guided cleavage of *ZmPHT1*s.

Overexpression of *PILNCR2* increases low-Pi tolerance in maize

The low Pi–inducible expression of *PILNCR2* and its co-localization with *ZmPHT1*s prompted us to analyze the potential role of *PILNCR2* in low-Pi tolerance. We generated transgenic maize that overexpressed *PILNCR2* (*PILNCR2-OE)* under the constitutive maize ubiquitin promoter. Two independent transgenic events were chosen on the basis of *PILNCR2* expression (Figure 4A). Overexpression of *PILNCR2* significantly increased maize fresh weight under both Pi-sufficient and Pi-deficient conditions (Figure 4B). After plants were subjected to a low-Pi treatment for 13 days, the fresh weight of old leaves (first, second, and third leaves from the bottom) decreased by 31% for WT plants but only by 5%–9% for *PILNCR2*-OE transgenic maize plants

(B) Detection of the *PILNCR2* lncRNA and *ZmPHT1*;*1*, *ZmPHT1*;*3*, *ZmPHT1*;*13,* or *ZmPHO2–5′ UTR* duplex using an endogenous ribonuclease protection assay. *GAPDH* mRNA and the *PILNCR2* region that did not overlap with *ZmPHT1s*/*ZmPHO2–5′ UTR* were used as controls. The primer locations are presented in the diagram.

(C) Relative mRNA levels of *ZmPHT1*s in *N. benthamiana* co-expressing *ZmMIR399b*, *ZmPHT1*s, *PILNCR2*, *PILNCR2-mut1* (mismatch), and *PILNCR2-mut2* (deletion) constructs. Real-time RT–PCR quantifications were normalized to the expression of tobacco 18S rRNA. Error bars represent standard errors (n = 3). Means with the same letter are not significantly different at $p < 0.05$ according to one-way ANOVA followed by Tukey's multiple comparison test.

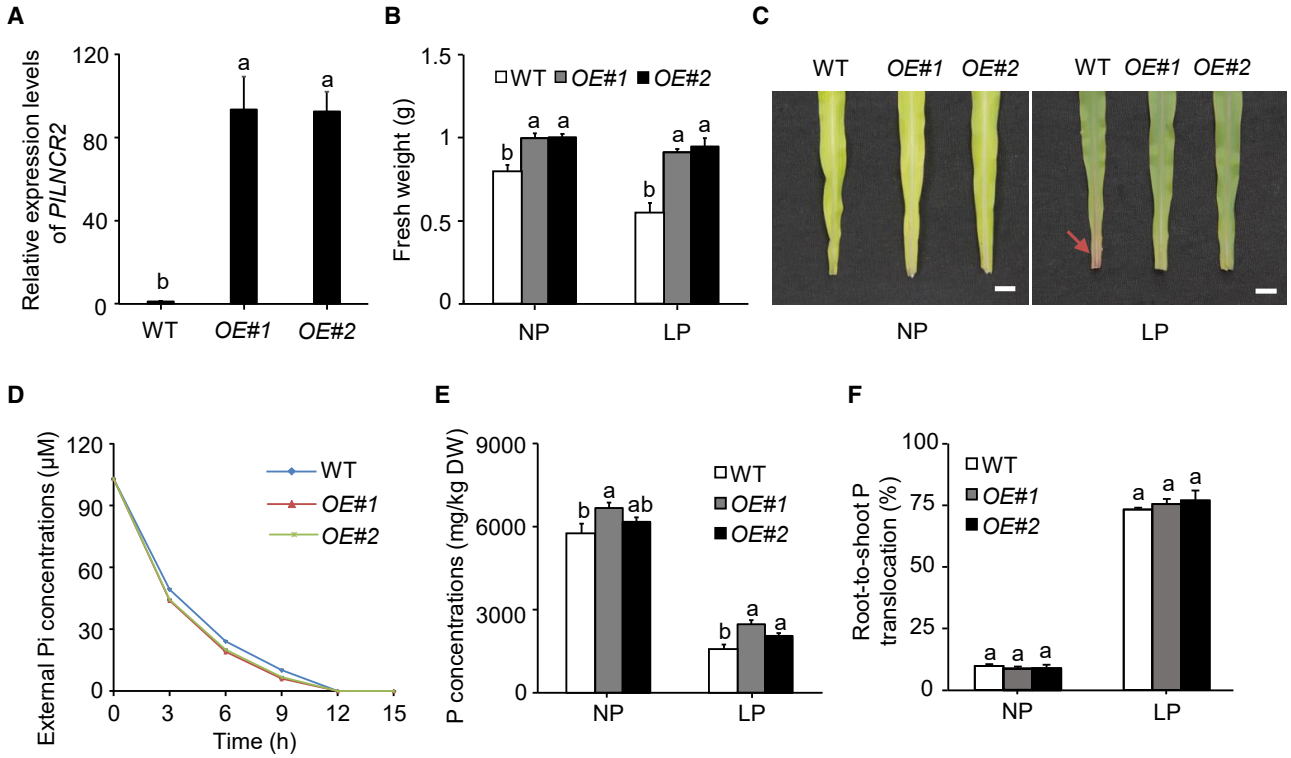

Figure 4. Transgenic maize plants overexpressing *PILNCR2* are more tolerant to low-Pi stress.

(A) Detection of *PILNCR2* mRNA abundance in *PILNCR2*-overexpressing transgenic maize by real-time RT–PCR. qRT–PCR quantifications were normalized to the expression of *ZmActin1*. Error bars represent standard errors of three biological replicates.

(B) Shoot fresh weight of old leaves (first, second, and third from bottom) from inbred line KN5585 (WT) and *PILNCR2*-overexpressing transgenic maize under normal- and low-Pi conditions. Values are means ± standard errors (n = 10).

(C) A representative photograph of *PILNCR2*-overexpressing transgenic maize grown under normal- and low-Pi conditions. Scale bars: 1 cm. The red arrows indicate the Pi-deficient phenotype.

(D) Pi uptake rates of KN5585 and *PILNCR2*-overexpressing transgenic maize. Error bars represent standard errors of three biological replicates. Each replicate included two plants.

(E) P concentrations in the roots of KN5585 and *PILNCR2*-overexpressing transgenic maize under normal- and low-Pi conditions.

(F) Root-to-shoot P translocation in KN5585 and *PILNCR2*-overexpressing transgenic maize under normal- and low-Pi conditions. Error bars represent standard errors of three biological replicates.

Means with the same letter in **(A)**, **(B)**, **(E),** and **(F)** are not significantly different at $p < 0.05$ according to one-way ANOVA followed by Tukey's multiple-comparison test. NP, normal Pi; LP, low Pi; FW, fresh weight; DW, dry weight.

(Figure 4B). Accumulation of the purple flavonoid pigment anthocyanin was observed in older leaves of WT plants but not of *PILNCR2*-OE transgenic maize plants (Figure 4C). These results suggested that overexpression of *PILNCR2* increases low-Pi tolerance in maize.

PILNCR2 interference with miRNA399-guided cleavage of *ZmPHT1* mRNAs suggested that *PILNCR2* might affect Pi uptake of maize. To test this hypothesis, we performed a Pi depletion assay in which the quantity of Pi remaining in a hydroponic solution (the external Pi) was measured after the growth of maize seedlings. The external Pi was exhausted much more rapidly by *PILNCR2*-OE transgenic maize than by WT maize (Figure 4D). Consistent with these results, P concentrations in roots and shoots were much higher in *PILNCR2*-OE transgenic maize than in the WT under both Pi-sufficient and Pi-deficient conditions (Figure 4E; Supplemental Figure 9). By contrast, root-to-shoot translocation of P was similar in *PILNCR2*-OE transgenic maize and the WT under both Pi-sufficient and Pi-deficient conditions (Figure 4F).

Knockout and knockdown of *PILNCR2* decreases low-Pi tolerance in maize

To further characterize the function of *PILNCR2* in low-P tolerance, we used the CRISPR–Cas9 system to generate *PILNCR2* loss-of function mutants (knockouts [*KO*s]). Because *PILNCR2* is an lncRNA, two single guide RNAs located on both sides of the transcription start site (TSS) were designed to destroy the binding site of RNA polymerase II (Supplemental Figure 10A). A total of 16 transgenic events were obtained and were found to have the same genotype (Supplemental Figure 10B). *PILNCR2* expression was not detected in *KO* transgenic maize by northern blot analysis (Figure 5A), demonstrating that the strategy to construct *KO* transgenic maize was effective. Cas9-free transgenic plants were used for phenotypic analysis. After the plants were subjected to a low-Pi treatment for 11 days, accumulation of the purple flavonoid pigment anthocyanin was observed in old leaves of *KO* transgenic maize but not in those of WT plants (Figure 5B). The external Pi was exhausted much more slowly by *KO* transgenic maize than by WT maize

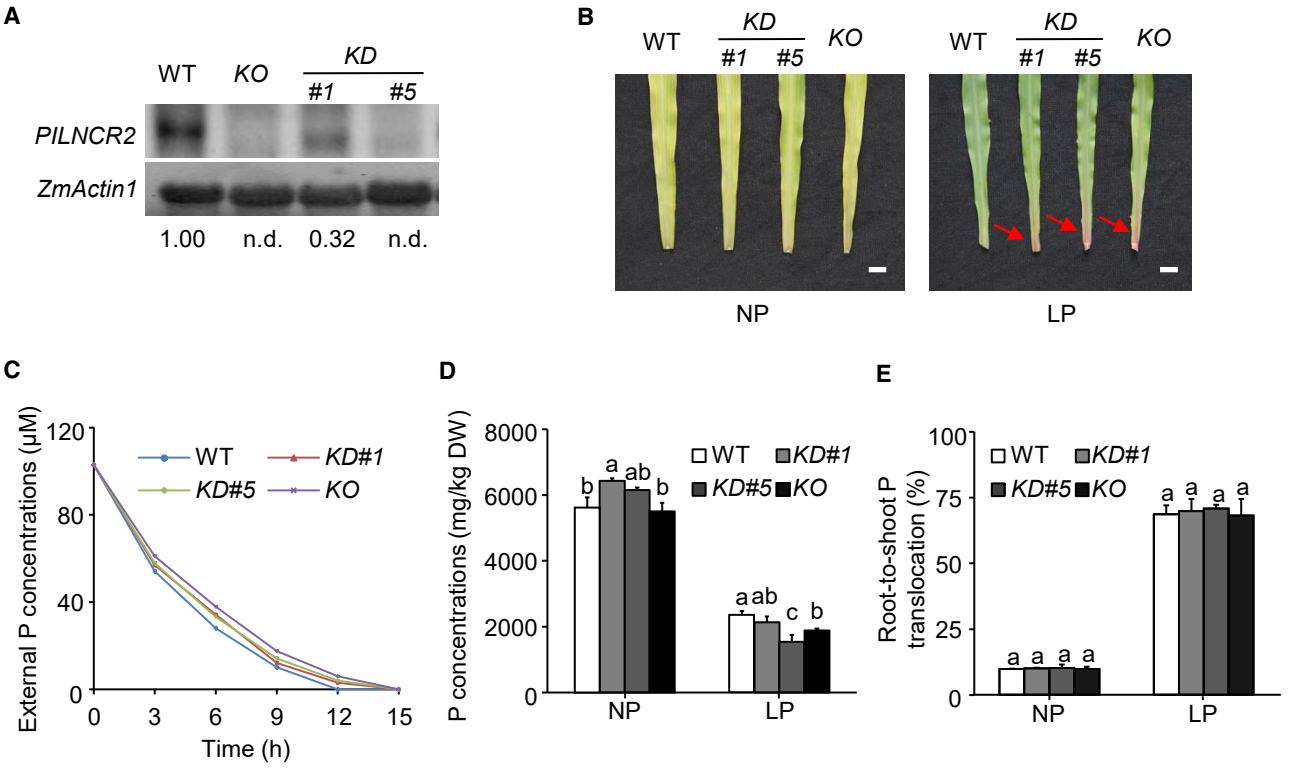

Figure 5. Transgenic maize plants with *PILNCR2* knockdown or knockout are more sensitive to low-Pi stress.

(A) Detection of *PILNCR2* mRNA abundance in *PILNCR2*-knockdown and -KO transgenic maize by northern blotting. *ZmActin1* was used as a loading control.

(B) A representative photograph of *PILNCR2*-knockdown and -KO transgenic maize grown under normal- and low-Pi conditions. Scale bars: 1 cm. The red arrows indicate the Pi-deficient phenotype.

(C) Pi uptake rate of KN5585 (WT) and *PILNCR2*-knockdown and -KO transgenic maize. Error bars represent standard errors of three biological replicates. Each replicate included two plants.

(D) P concentrations in the roots of KN5585 and *PILNCR2*-knockdown and -KO transgenic maize under normal- and low-Pi conditions.

(E) Root-to-shoot P translocation in KN5585 and *PILNCR2*-knockdown and -KO transgenic maize under normal- and low-Pi conditions. Means with the same letter are not significantly different at $p < 0.05$ according to one-way ANOVA followed by Tukey's multiple comparison test. NP, normal Pi; LP, low Pi; FW, fresh weight; DW, dry weight.

(Figure 5C). P concentrations in roots and shoots were much lower in *KO* transgenic maize than in the WT under Pi-deficient conditions (Figure 5D; Supplemental Figure 11).

Because there was only one genotype in the *KO* transgenic events, an artificial miRNA targeting *PILNCR2* was designed according to the strict base-pairing rules (Schwab et al., 2006) and introduced into maize. The effectiveness of *PILNCR2* destruction was verified by northern blot analysis, and two independent knockdown lines (*KD#1* and *KD#5*) were chosen for subsequent analysis (Figure 5A). Consistent with observations in *KO* transgenic maize, anthocyanin pigmentation appeared earlier in *KD* transgenic maize than in WT maize (Figure 5B). We also observed a slower exhaustion of external Pi and lower P concentrations in roots and shoots of *KD* transgenic maize than in those of the WT under Pi-deficient conditions (Figure 5C and 5D; Supplemental Figure 11). KO or KD of *PILNCR2* did not affect root-to-shoot translocation of P in maize under either Pi-sufficient or Pi-deficient conditions (Figure 5E). These results showed that repressing the abundance of *PILNCR2* mRNA reduced low-Pi tolerance in maize.

Pi-toxicity phenotype disappears in MIR399b-OE/PILNCR2-KO *double transgenic maize*

In a previous study in our laboratory, *ZmMIRNA399b*-OE transgenic maize had typical P-toxicity phenotypes (with chlorosis or necrosis at the leaf tips and margins of old leaves) under Pi-sufficient conditions, and the P-toxicity phenotypes were due to downregulation of *ZmPHO2* (Du et al., 2018). To determine whether the effects of *PILNCR2* on tolerance of maize to low-Pi conditions involve ZmmiRNA399, we generated *ZmMIRNA399b-OE* and *PILNCR2*-KO double transgenic maize by cross breeding (Figure 6A). In contrast to *ZmMIRNA399b*-OE transgenic maize, *ZmMIRNA399b-OE/PILNCR2-KO* double transgenic maize did not exhibit typical Pi-toxicity phenotypes (Figure 6B). Consistent with the latter observation, Pi did not accumulate in shoots of *MIR399b-OE/PILNCR2-KO* double transgenic maize (Figure 6C). These results suggested that the function of *PILNCR2* in maize tolerance to low-Pi conditions involves ZmmiRNA399.

Transcript levels of *PILNCR2* do not affect *MIR399b* and *PHO2* mRNA abundance

To further characterize the possible relationship between *PILNCR2* and ZmmiRNA399, we tested whether *PILNCR2*

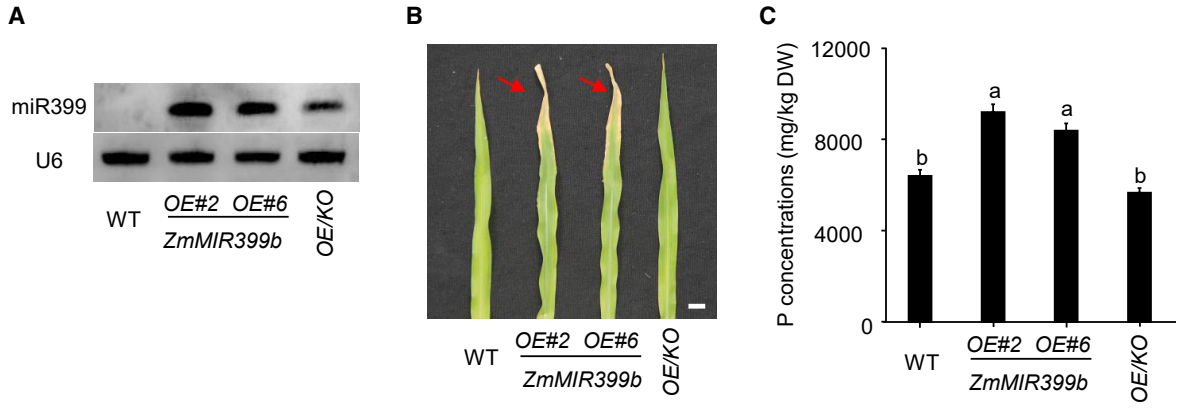

Figure 6. Phenotypes of *MIR399b-OE*/*PILNCR2-KO* double transgenic maize grown in hydroponic solution.

(A) Detection of ZmmiRNA399 abundance in WT, *MIR399b-OE*, and *MIR399b-OE*/*PILNCR2-KO* double transgenic maize. U6 was used as a loading control.

(B) A representative photograph of *MIR399b-OE*/*PILNCR2-KO* double transgenic maize grown under Pi-sufficient conditions. Scale bars: 1 cm. The red arrows indicate the Pi-toxicity phenotype.

(C) P concentrations in old leaves of WT, *MIR399b-OE*, and *MIR399b-OE*/*PILNCR2-KO* double transgenic maize grown under Pi-sufficient conditions. Means with the same letter are not significantly different at $p < 0.05$ according to one-way ANOVA followed by Tukey's multiple comparison test. DW, dry weight.

transcript levels affected the expression of *MIR399b* and *PHO2*. To avoid the effects of endogenous *PILNCR2*, we used transgenic maize supplied with Pi. Overexpression or KO of *PILNCR2* did not affect the mRNA levels of *MIR399b* (Figure 7A), and *PHO2* expression increased significantly only in the *PILNCR2-OE#1* transgenic line (Figure 7A). Consistent with the phenotypes of *PILNCR2-OE* and *-KO* transgenic maize, the mRNA abundance of *ZmPHT1*;*3* and *ZmPHT1*;*13* was increased in *PILNCR2-OE* transgenic maize and reduced in *PILNCR2-KO* mutants (Figure 7A). Because *ZmPHT1*;*1* fully overlapped with *PILNCR2*, we detected its expression only in the *PILNCR2-KO* mutant. Similar to *ZmPHT1*;*3* and *ZmPHT1*;*13*, *ZmPHT1*;*1* showed reduced expression in *PILNCR2-KO* mutants (Figure 7A).

We also tested the effects of ZmmiRNA399 on the expression of *PILNCR2* and *PHO2*. Consistent with our previous results (Du et al., 2018), overexpression of *MIR399b* reduced the mRNA abundance of *PHO2* (Figure 7B). By contrast, overexpression of *MIR399b* did not affect the mRNA abundance of *PILNCR2* (Figure 7B). Compared with their expression in *MIR399b-OE* transgenic maize, the expression of *ZmPHT1*;*1*, *ZmPHT1*;*3*, and *ZmPHT1*;*13* was significantly downregulated in *ZmMIRNA399b-OE* and *PILNCR2-KO* double transgenic maize (Figure 7B). These results further suggested that *PILNCR2* interferes with the miRNA399-guided cleavage of *ZmPHT1* mRNAs.

DISCUSSION

Regulation of *ZmPHT1s* by ZmmiRNA399

In *Arabidopsis* and rice, miRNA399 has been demonstrated to confer P homeostasis by suppressing the expression of *PHO2* (Fujii et al., 2005; Chiou et al., 2006; Hu et al., 2011). Using *ZmMIRNA399b*-OE transgenic maize and transient expression analysis in *N. benthamiana*, previous work in our laboratory showed that *ZmPHO2* is post-transcriptionally regulated by miR399. In the present research, we verified that *ZmPHT1*;*1*, *ZmPHT1*;*3*, and *ZmPHT1*;*13* are the authentic targets of ZmmiRNA399. That conclusion was based on the following evidence: (1) penalty points between ZmmiRNA399 and *ZmPHT1*;*1*/*ZmPHT1*;*3*/*ZmPHT1*;*13* ranged from 3 to 3.5 and did not exceed the criteria for identifying a miRNA target (Schwab et al., 2005); (2) the mRNA abundances of *ZmPHT1*;*1*, *ZmPHT1*;*3*, and *ZmPHT1*;*13* were repressed when these genes were co-expressed with *ZmMIRNA399b* in *N. benthamiana*; (3) overexpression of *MIRNA399b* reduced the mRNA levels of *ZmPHT1*;*1*, *ZmPHT1*;*3,* and *ZmPHT1*;*13* in maize; and (4) the cleavage sites in *ZmPHT1*;*1*, *ZmPHT1*;*3,* and *ZmPHT1*;*13* were mapped by 5′-RACE.

Pi uptake is an energy-requiring process that involves Pi translocation from the rhizosphere into the root cells via Pi/H^+ co-transport (Liu et al., 2014). Under Pi-deficient conditions, the expression levels of *PHT*s were significantly induced. To sustain essential physiological and biochemical processes, plants should maintain optimum *PHT* mRNA levels in order to balance Pi acquisition and normal development. We inferred that miRNA399-guided repression of *ZmPHT1*s is responsible for maintaining the balance between Pi acquisition and normal plant development under Pi-deficient conditions.

The relationship between *PILNCR2* and *ZmmiRNA399* in maize

PILNCR2 was transcribed from the opposing DNA strand of *ZmPHT1*;*1* and formed *cis*-natural antisense transcripts (NATs) with *ZmPHT1*;*1*. More than 91% of *cis*-NATs are lncRNAs (Wang et al., 2014a, 2014b), but few of these *cis*-NATs have been functionally characterized in detail in plants (Reis and Poirier, 2021). These previously identified lncRNAs control gene expression at various levels by modifying chromatin accessibility, transcription, splicing, and translation (Wierzbicki et al., 2021). Researchers have suggested that miRNA activity could be affected by lncRNAs, such as mimic miRNA targets (Franco-Zorrilla et al., 2007). *cis*-NATs are

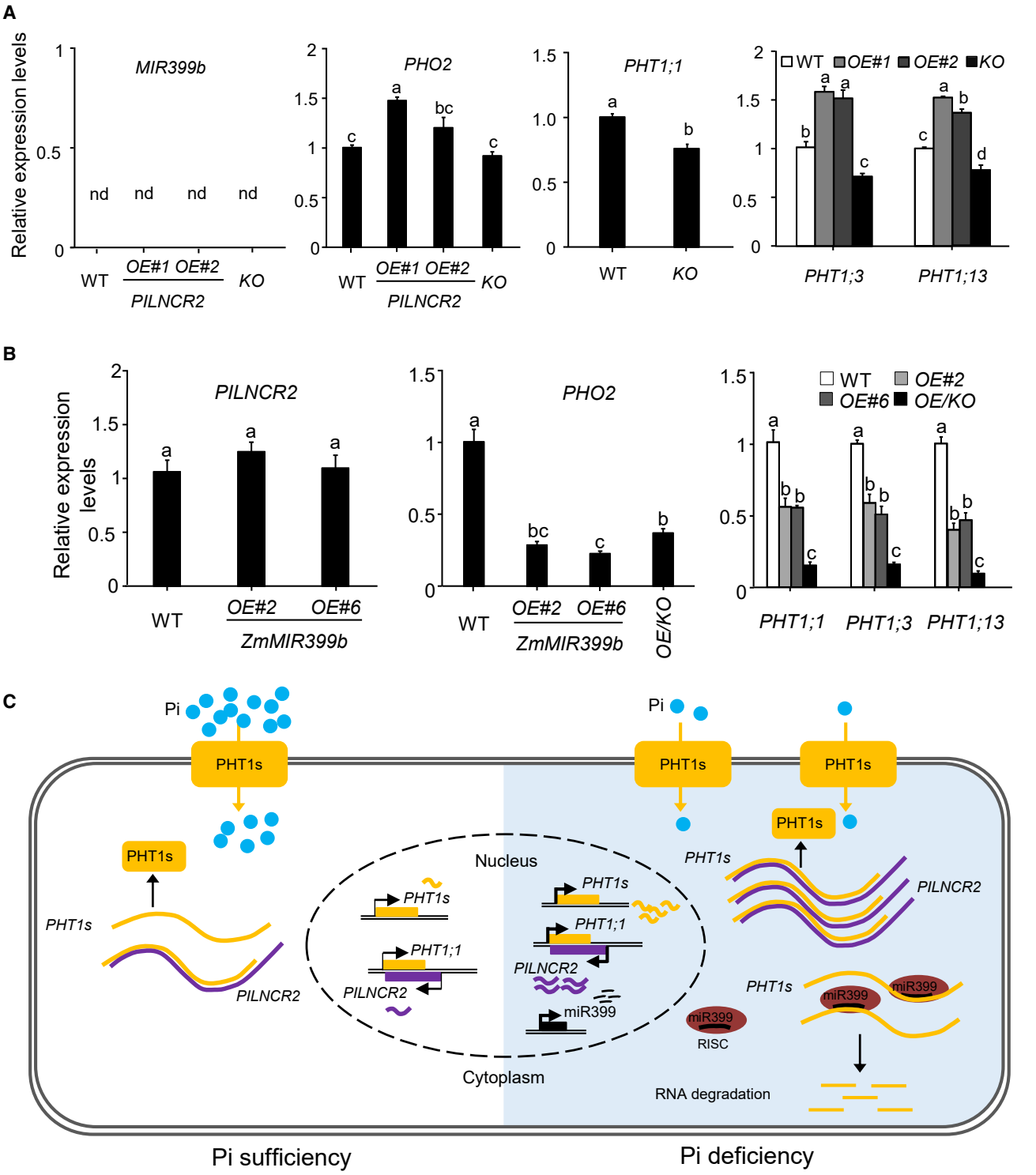

Figure 7. *PILNCR2* abundance does not affect *MIR399b* and *PHO2* transcripts.

(A) The effects of *PILNCR2* abundance on *MIR399b*, *PHO2*, *PHT1*;*1*, *PHT1*;*3*, and *PHT1*;*13* transcripts.

(B) The effects of *MIR399b* abundance on *PILNCR2*, *PHO2*, *PHT1*;*1*, *PHT1*;*3*, and *PHT1*;*13* transcripts. Quantifications were normalized to the expression of *ZmActin1*. Error bars represent standard errors of three biological replicates.

Means with the same letter in **(A)** and **(B)** are not significantly different at $p < 0.05$ according to one-way ANOVA followed by Tukey's multiple comparison test.

(C) A proposed model illustrating the role of *PILNCR2* in determining maize tolerance to low Pi. *PILNCR2* interferes with miRNA399-guided cleavage of *ZmPHT1* mRNAs to regulate Pi homeostasis in maize.

often thought to form double-stranded RNA stretches, triggering gene silencing (Reis and Poirier, 2021). Previous results from our laboratory also showed that siRNAs originating from the OR of a gene pair could regulate the biogenesis of miRNA169 in *Arabidopsis* (Gao et al., 2015). However, growing evidence suggests that compared with non-overlapping mRNAs, *cis*-NATs are not major sources of siRNAs (Henz et al., 2007). In the present research, we identified *PILNCR2* from our lncRNA libraries. *PILNCR2* has a poly-A tail and cap structure and is located in the cytoplasm. No siRNAs were detected in the OR of *PILNCR2* or *ZmPHT1*;*1*. In the cytoplasm, *PILNCR2* can form an RNA/RNA duplex with *ZmPHT1*;*1*, *ZmPHT1*;*3*, or *ZmPHT1*;*13*. This RNA/RNA duplex could interrupt base pairing between ZmmiRNA399 and *ZmPHT1*;*1*, *ZmPHT1*;*3*, or *ZmPHT1*;*13*. As a consequence, the *ZmPHT1*;*1*, *ZmPHT1*;*3*, or *ZmPHT1*;*13* mRNA protected by *PILNCR2* would not be cleaved by ZmmiRNA399. This regulatory model might apply to other *cis*-NATs with positive correlations.

The function of *PILNCR2* in low-P tolerance of maize

In previous studies, transgenic *Arabidopsis* plants overexpressing miR399 accumulated excessive Pi in shoots and displayed Pi-toxicity symptoms that resembled the phenotypes of the *pho2* mutant (Aung et al., 2006; Chiou et al., 2006; Hu et al., 2011). *PHO2* encodes a ubiquitin E2 conjugase and modulates the protein degradation of PHO1, PHT1;1, PHT1;2, PHT1;3, and PHT1;4 to maintain Pi homeostasis in *Arabidopsis* (Liu et al., 2012; Huang et al., 2013). Further research indicated the importance of the miR399–PHO2 pathway for regulating plant adaptive responses to Pi deficiency (Hu et al., 2011; Du et al., 2018). Here, we found that *PILNCR2* forms a different pathway with miR399 to regulate low-Pi tolerance in maize. This conclusion is supported by the following evidence from the current study: (1) overexpression of *PILNCR2* increases low-Pi tolerance in maize, (2) KO and KD of *PILNCR2* decrease low-Pi tolerance in maize, and (3) the Pi-toxicity phenotype is absent in *MIR399b-OE*/*PILNCR2-KO* double transgenic maize under Pi-sufficient conditions. We therefore propose the following model for how *PILNCR2* and *ZmmiRNA399* function together to increase low-Pi tolerance in maize (Figure 7C). The expression levels of both *PILNCR2* and ZmmiRNA399 are upregulated by Pi deficiency. In the cytoplasm, some *ZmPHT1*;*1*, *ZmPHT1*;*3*, or *ZmPHT1*;*13* forms RNA/RNA duplexes with *PILNCR2*. The *ZmPHT1*;*1*, *ZmPHT1*;*3*, or *ZmPHT1*;*13* in the duplexes is not cleaved by ZmmiRNA399 and contributes to the balance between Pi acquisition and normal development of maize under Pi-deficient conditions. Taken together, our results provide a new model for how lncRNAs affect miRNA functions in plants.

METHODS

Plant materials and growth conditions

Seed pre-treatment and germination were performed as described previously (Sun et al., 2018). When the first leaf from the bottom of a seedling was fully expanded, the endosperm was removed. The seedlings were then transferred to 3-L containers (three seedlings per container) filled with hydroponic solution. The hydroponic solution was half-strength Hoagland's nutrient solution for the first 2 days and full-strength Hoagland's nutrient solution with 250 μM PO_4^{3-} (control) or 5 μM (low-P) PO_4^{3-} thereafter. The other components of the hydroponic solutions were similar to those described by Du et al. (2018). The containers were placed randomly in a culture room (14-h light/10-h dark and 28°C/22°C day/night), where their positions were changed frequently. The hydroponic solution was replaced with fresh solution every 2 days to ensure pH stability.

Generation of transgenic maize

To generate *PILNCR2*-OE transgenic maize, a 2450-bp fragment containing the OR with *ZmPHT1*;*1* was amplified and cloned into the pCUB vector under the control of the maize ubiquitin promoter using the *Bam*HI restriction site via an In-Fusion reaction.

To generate a *PILNCR2* loss-of function mutant, CRISPR–Cas9-mediated editing of *PILNCR2* was performed as described by Xing et al. (2014). Because *PILNCR2* is an lncRNA, two single guide RNAs located at −1050 and 637 bp of the TSS were designed to destroy the binding site of RNA polymerase (Supplemental Figure 10A). The fragments were cloned into the pBUE411 vector.

To generate *PILNCR2*-KD transgenic maize, we designed an artificial miRNA targeting 458–479 bp of the *PILNCR2* TSS and engineered it into the pRS300 vector by replacing the original *MIR319a* sequence (Supplemental Figure 10A; Schwab et al., 2006).

The plasmids were electroporated into *Agrobacterium tumefaciens* EHA105, then transformed into the maize inbred line KN5585 at Forfuture Breeding Biotechnology (Changzhou, China). Positive transgenic events were selected as described previously (Sun et al., 2018). T_2 or T_3 homozygous lines were used for the experiments.

RNA analysis

Extraction and purification of total RNA, synthesis of first-strand cDNA, qPCR, and stem-loop qRT–PCR were performed as described previously by Du et al. (2018). qPCR was performed on an ABI 7500 system (Applied Biosystems) using SYBR Select Master Mix (Applied Biosystems). The comparative cycle threshold method was used with two different controls, and each experiment was replicated three times.

Small RNA was separated from total RNA by PEG precipitation. The loading, fractionation, probe labeling, and detection of small RNA were performed as reported previously (Gao et al., 2015). The primers used in this experiment are listed in Supplemental Table 2.

Rapid amplification of cDNA ends

To determine the transcriptional start and termination sites of *PILNCR2*, 5′- and 3′-RACE PCR was carried out using the SMARTer RACE kit (Clontech). To obtain the cleavage transcripts, total RNA was extracted from maize roots that had been subjected to Pi deficiency for 6 days. 5′-RACE PCR was carried out according to the manufacturer's instructions (Thermo Fisher Scientific). RACE fragments were cloned and sequenced after gel purification.

To determine whether maize contains capped-*PILNCR2* transcripts, the extracted RNA was treated with or without calf intestine alkaline phosphatase. Afterward, all samples were treated with tobacco acid pyrophosphatase (Ariel et al., 2014) before 5′-RACE was carried out according to the manufacturer's instructions (Thermo Fisher Scientific).

Preparation of nuclear and cytoplasmic extracts

Nuclear/cytoplasmic fractionation was performed as described previously by Zhao et al. (2018) and Csorba et al. (2014). In brief, root samples were ground into fine powder and lysed in 2 volumes of 20 mM Tris–HCl (pH 7.4), 25% glycerol, 20 mM KCl, 2 mM EDTA, 2.5 mM $MgCl_2$, 250 mM sucrose, 5 mM DTT, and 40 U/ml RNase inhibitor. After

centrifugation at 13 000 × *g* for 10 min at 4°C, the supernatant was collected as a cytosolic extract. The pellet was washed with NRBT buffer (20 mM Tris–HCl [pH 7.4], 25% glycerol, 2.5 mM $MgCl_2$, 0.2% Triton X-100, 5 mM DTT, and 160 U/ml RNase inhibitor) until it became white. The pellets were resuspended in 20 mM Tris–HCl (pH 7.5), 200 mM KCl, 2 mM DTT, and 1% Triton X-100 and were collected as nuclear extracts.

RNA–RNA *in vitro* interaction

An RNA–RNA *in vitro* interaction assay was performed as described previously (Zhang et al., 2018). In brief, a 25-μl volume of Protein A/G Magnetic Beads (Pierce) was incubated with anti-BrdU monoclonal antibody or immunoglobulin G antibody for 2 h at 4°C before the beads were washed twice with RIP Wash Buffer (Millipore). The beads were then resuspended in RIP Wash Buffer containing 17.5 mM EDTA and 40 U/ml RNase Inhibitor. A 5 pmol concentration of BrU-labeled RNAs (*PILNCR2* fragments overlapping or not overlapping with *PHT1*;*1*) was added and incubated with beads for 2 h at 4°C. *ZmPHT1*;*1*, *ZmPHT1*;*3*, or *ZmPHT1*;*13* was then added, and the preparation was incubated overnight at 4°C. After the preparation was digested in RIP Wash Buffer containing 1.2 μg/μl proteinase K and 1% SDS, RNA was extracted. qRT–PCR was performed as described in the RNA analysis section.

Endogenous ribonuclease protection assay

The RNA duplex was detected by an endogenous ribonuclease protection assay (Gilman, 2001). Total RNA was extracted from maize roots that had been subjected to low-Pi stress for 8 days. DNase I and RPA-grade RNase A were then added to remove the genomic DNA and single-stranded RNAs. The residual endogenous double-stranded RNAs were isolated, and RT–PCR was performed as described in the RNA analysis section.

In situ hybridization

The specific fragments of *PILNCR2* that did not overlap with *ZmPHT1*;*1* (187 bp), *ZmPHT1*;*1* (179 bp), *ZmPHT1*;*3* (188 bp), and *ZmPHT1*;*13* (236 bp) were amplified by PCR. The amplified fragments were cloned into the pGEM-T-easy vector (Promega). The corresponding probes were generated by *in vitro* transcription using T_7 RNA polymerases and labeled with digoxigenin according to the manufacturer's instructions (Roche). To avoid the effects of endogenous *PILNCR2*, *PILNCR2*-KO transgenic maize were used for detecting the expression patterns of *ZmPHT1*s. The roots of WT or *PILNCR2-KO* were fixed in formalin and infiltrated with paraffin. The *in situ* hybridization was performed as described previously (Sun et al., 2018).

Transient expression in maize protoplasts

Maize leaf protoplasts were prepared as described previously (Du et al., 2018). The predicted potential ORF1, ORF2, ORF3, and ORF4 in *PILNCR2* were amplified and cloned into the NL vector, which was fused to a GFP protein in the N or C terminus using the *Bam*HI restriction site via an In-Fusion reaction. The expression plasmids were transiently expressed in maize mesophyll protoplasts as described previously (Du et al., 2018). Images were collected with a Zeiss LSM700 confocal microscope.

Transient expression in *N. benthamiana*

The cDNA sequences of *PILNCR2* overlapping with *ZmPHT1*;*1*, *ZmPHT1*;*1*, and *ZmMIRNA399b* were amplified with the primers listed in Supplemental Table 2. The amplified fragments were cloned into the pCPB vector and electroporated into *Agrobacterium tumefaciens* strain 3101.

Overnight cultures were harvested and mixed at a 1:1 ratio in various combinations. The plasmids were transiently expressed in *N. benthamiana* epidermal cells as described by Du et al. (2018). Leaves were harvested 2 days after infiltration and subjected to RNA analysis as described earlier.

Pi depletion assay

Two seedlings were transferred to a flask with 300 ml depletion solution. The components in the depletion solution were similar to those described by Wang et al. (2020). A sample (1 ml) of the depletion solution was collected every 3 h, and the Pi content was determined by inductively coupled plasma optical emission spectroscopy (OPTIMA 3300 DV, PerkinElmer, Waltham, MA, USA).

Determination of total P content

Samples were pre-treated as described previously (Du et al., 2018). In brief, shoots and roots were heated to 105°C for 30 min and then dried to constant weight at 60°C. The dried samples were milled to a fine powder and weighed. The samples were then digested with HNO_3–H_2O_2 in a microwave-accelerated reaction system (CEM, Matthews, NC, USA) until the solution became clear. The total P content was determined by inductively coupled plasma optical emission spectroscopy (OPTIMA 3300 DV, PerkinElmer).

SUPPLEMENTAL INFORMATION

Supplemental information is available at *Molecular Plant Online*.

FUNDING

This work was supported by the National Key Research and Development Program of China (2021YFF1000500) and the Agricultural Science and Technology Innovation Program of CAAS to W.-X.L.

AUTHOR CONTRIBUTIONS

W.-X.L. designed the research and wrote the article. Y.W. and Z.W. performed the experiments. Q.D. performed bioinformatic analysis. K.W. examined the cleavage sites. C.Z. determined the P content.

ACKNOWLEDGMENTS

No conflict of interest is declared.

Received: July 28, 2022
Revised: March 26, 2023
Accepted: May 29, 2023
Published: June 1, 2023

REFERENCES

Ameres, S.L., Martinez, J., and Schroeder, R. (2007). Molecular basis for target RNA recognition and cleavage by human RISC. Cell **130**:101–112.

Ariel, F., Jegu, T., Latrasse, D., Romero-Barrios, N., Christ, A., Benhamed, M., and Crespi, M. (2014). Noncoding transcription by alternative RNA polymerases dynamically regulates an auxin-driven chromatin loop. Mol. Cell **55**:383–396.

Aung, K., Lin, S.I., Wu, C.C., Huang, Y.T., Su, C.L., and Chiou, T.J. (2006). pho2, a phosphate overaccumulator, is caused by a nonsense mutation in a microRNA399 target gene. Plant Physiol. **141**:1000–1011.

Baumberger, N., and Baulcombe, D.C. (2005). Arabidopsis ARGONAUTE1 is an RNA Slicer that selectively recruits microRNAs and short interfering RNAs. Proc. Natl. Acad. Sci. USA **102**:11928–11933.

Chiou, T.J., Aung, K., Lin, S.I., Wu, C.C., Chiang, S.F., and Su, C.L. (2006). Regulation of phosphate homeostasis by microRNA in Arabidopsis. Plant Cell **18**:412–421.

Csorba, T., Questa, J.I., Sun, Q., and Dean, C. (2014). Antisense COOLAIR mediates the coordinated switching of chromatin states at FLC during vernalization. Proc. Natl. Acad. Sci. USA **111**:16160–16165.

Dai, X., Zhuang, Z., and Zhao, P.X. (2018). psRNATarget:a plant small RNA target analysis server (2017 release). Nucleic Acids Res. **46**:W49–W54.

Das, D., Paries, M., Hobecker, K., Gigl, M., Dawid, C., Lam, H.M., Zhang, J., Chen, M., and Gutjahr, C. (2022). PHOSPHATE STARVATION RESPONSE transcription factors enable arbuscular mycorrhiza symbiosis. Nat. Commun. **13**:477.

Du, Q., Wang, K., Xu, C., Zou, C., Xie, C., Xu, Y., and Li, W.X. (2016). Strand-specific RNA-Seq transcriptome analysis of genotypes with and without low phosphorus tolerance provides novel insights into phosphorus-use efficiency in maize. BMC Plant Biol. **16**:222.

Du, Q., Wang, K., Zou, C., Xu, C., and Li, W.X. (2018). The PILNCR1-miRNA399 regulatory module is important for low phosphate tolerance in maize. Plant Physiol. **177**:1743–1753.

Franco-Zorrilla, J.M., Valli, A., Todesco, M., Mateos, I., Puga, M.I., Rubio-Somoza, I., Leyva, A., Weigel, D., García, J.A., and Paz-Ares, J. (2007). Target mimicry provides a new mechanism for regulation of microRNA activity. Nat. Genet. **39**:1033–1037.

Fujii, H., Chiou, T.J., Lin, S.I., Aung, K., and Zhu, J.K. (2005). A miRNA involved in phosphate-starvation response in Arabidopsis. Curr. Biol. **15**:2038–2043.

Gao, W., Liu, W., Zhao, M., and Li, W.X. (2015). NERF encodes a RING E3 ligase important for drought resistance and enhances the expression of its antisense gene NFYA5 in Arabidopsis. Nucleic Acids Res. **43**:607–617.

Gilman, M. (2001). Ribonuclease protection assay. Curr. Protoc. Mol. Biol. **Chapter 4**:Unit4.7.

Guo, M., Ruan, W., Zhang, Y., Zhang, Y., Wang, X., Guo, Z., Wang, L., Zhou, T., Paz-Ares, J., and Yi, K. (2022). A reciprocal inhibitory module for Pi and iron signaling. Mol. Plant **15**:138–150.

Henz, S.R., Cumbie, J.S., Kasschau, K.D., Lohmann, J.U., Carrington, J.C., Weigel, D., and Schmid, M. (2007). Distinct expression patterns of natural antisense transcripts in Arabidopsis. Plant Physiol. **144**:1247–1255.

Heo, J.B., and Sung, S. (2011). Vernalization-mediated epigenetic silencing by a long intronic noncoding RNA. Science **331**:76–79.

Hu, B., Zhu, C., Li, F., Tang, J., Wang, Y., Lin, A., Liu, L., Che, R., and Chu, C. (2011). LEAF TIP NECROSIS1 plays a pivotal role in the regulation of multiple phosphate starvation responses in rice. Plant Physiol. **156**:1101–1115.

Huang, T.K., Han, C.L., Lin, S.I., Chen, Y.J., Tsai, Y.C., Chen, Y.R., Chen, J.W., Lin, W.Y., Chen, P.M., Liu, T.Y., et al. (2013). Identification of downstream components of ubiquitin-conjugating enzyme PHOSPHATE2 by quantitative membrane proteomics in Arabidopsis roots. Plant Cell **25**:4044–4060.

Ingolia, N.T., Lareau, L.F., and Weissman, J.S. (2011). Ribosome profiling of mouse embryonic stem cells reveals the complexity and dynamics of mammalian proteomes. Cell **147**:789–802.

Jabnoune, M., Secco, D., Lecampion, C., Robaglia, C., Shu, Q., and Poirier, Y. (2013). A rice cis-natural antisense RNA acts as a translational enhancer for its cognate mRNA and contributes to phosphate homeostasis and plant fitness. Plant Cell **25**:4166–4182.

Kindgren, P., Ard, R., Ivanov, M., and Marquardt, S. (2018). Transcriptional read-through of the long non-coding RNA SVALKA governs plant cold acclimation. Nat. Commun. **9**:4561.

Kleaveland, B., Shi, C.Y., Stefano, J., and Bartel, D.P. (2018). A network of noncoding regulatory RNAs acts in the mammalian brain. Cell **174**:350–362.e17.

Lambers, H. (2022). Phosphorus acquisition and utilization in plants. Annu. Rev. Plant Biol. **73**:17–42.

Liu, F., Xu, Y., Jiang, H., Jiang, C., Du, Y., Gong, C., Wang, W., Zhu, S., Han, G., and Cheng, B. (2016). Systematic identification, evolution and expression analysis of the *Zea mays* PHT1 gene family reveals several new members involved in root colonization by arbuscular mycorrhizal fungi. Int. J. Mol. Sci. **17**:930.

Liu, T.Y., Huang, T.K., Tseng, C.Y., Lai, Y.S., Lin, S.I., Lin, W.Y., Chen, J.W., and Chiou, T.J. (2012). PHO2-dependent degradation of PHO1 modulates phosphate homeostasis in Arabidopsis. Plant Cell **24**:2168–2183.

Liu, T.Y., Lin, W.Y., Huang, T.K., and Chiou, T.J. (2014). MicroRNA-mediated surveillance of phosphate transporters on the move. Trends Plant Sci. **19**:647–655.

López-Arredondo, D.L., Leyva-González, M.A., González-Morales, S.I., López-Bucio, J., and Herrera-Estrella, L. (2014). Phosphate nutrition: improving low-phosphate tolerance in crops. Annu. Rev. Plant Biol. **65**:95–123.

Minajigi, A., Froberg, J.E., Wei, C., Sunwoo, H., Kesner, B., Colognori, D., Lessing, D., Payer, B., Boukhali, M., Haas, W., and Lee, J.T. (2015). A comprehensive xist interactome reveals cohesin repulsion and an RNA-directed chromosome conformation. Science **349**:aab2276.

Paz-Ares, J., Puga, M.I., Rojas-Triana, M., Martinez-Hevia, I., Diaz, S., Poza-Carrión, C., Miñambres, M., and Leyva, A. (2022). Plant adaptation to low phosphorus availability: core signaling, crosstalks, and applied implications. Mol. Plant **15**:104–124.

Pei, L., Jin, Z., Li, K., Yin, H., Wang, J., and Yang, A. (2013). Identification and comparative analysis of low phosphate tolerance-associated microRNAs in two maize genotypes. Plant Physiol. Biochem. **70**:221–234.

Péret, B., Clément, M., Nussaume, L., and Desnos, T. (2011). Root developmental adaptation to phosphate starvation: better safe than sorry. Trends Plant Sci. **16**:442–450.

Reis, R.S., and Poirier, Y. (2021). Making sense of the natural antisense transcript puzzle. Trends Plant Sci. **26**:1104–1115.

Ried, M.K., Wild, R., Zhu, J., Pipercevic, J., Sturm, K., Broger, L., Harmel, R.K., Abriata, L.A., Hothorn, L.A., Fiedler, D., et al. (2021). Inositol pyrophosphates promote the interaction of SPX domains with the coiled-coil motif of PHR transcription factors to regulate plant phosphate homeostasis. Nat. Commun. **12**:384.

Schwab, R., Ossowski, S., Riester, M., Warthmann, N., and Weigel, D. (2006). Highly specific gene silencing by artificial microRNAs in *Arabidopsis*. Plant Cell **18**:1121–1133.

Schwab, R., Palatnik, J.F., Riester, M., Schommer, C., Schmid, M., and Weigel, D. (2005). Specific effects of microRNAs on the plant transcriptome. Dev. Cell **8**:517–527.

Song, X., Li, Y., Cao, X., and Qi, Y. (2019). MicroRNAs and their regulatory roles in plant-environment interactions. Annu. Rev. Plant Biol. **70**:489–525.

Sun, Q., Liu, X., Yang, J., Liu, W., Du, Q., Wang, H., Fu, C., and Li, W.X. (2018). MicroRNA528 affects lodging resistance of maize by regulating lignin biosynthesis under nitrogen-luxury conditions. Mol. Plant **11**:806–814.

Swiezewski, S., Liu, F., Magusin, A., and Dean, C. (2009). Cold-induced silencing by long antisense transcripts of an Arabidopsis polycomb target. Nature **462**:799–802.

Tian, W.H., Ye, J.Y., Cui, M.Q., Chang, J.B., Liu, Y., Li, G.X., Wu, Y.R., Xu, J.M., Harberd, N.P., Mao, C.Z., et al. (2021). A transcription factor STOP1-centered pathway coordinates ammonium and phosphate acquisition in Arabidopsis. Mol. Plant **14**:1554–1568.

Wang, H., Chung, P.J., Liu, J., Jang, I.C., Kean, M.J., Xu, J., and Chua, N.H. (2014a). Genome-wide identification of long noncoding natural antisense transcripts and their responses to light in Arabidopsis. Genome Res. **24**:444–453.

Wang, F., Cui, P.J., Tian, Y., Huang, Y., Wang, H.F., Liu, F., and Chen, Y.F. (2020). Maize ZmPT7 regulates Pi uptake and redistribution which is modulated by phosphorylation. Plant Biotechnol. J. **18**:2406–2419.

Wang, Y., Fan, X., Lin, F., He, G., Terzaghi, W., Zhu, D., and Deng, X.W. (2014b). Arabidopsis noncoding RNA mediates control of photomorphogenesis by red light. Proc. Natl. Acad. Sci. USA **111**:10359–10364.

Wang, Y., Luo, X., Sun, F., Hu, J., Zha, X., Su, W., and Yang, J. (2018). Overexpressing lncRNA LAIR increases grain yield and regulates neighbouring gene cluster expression in rice. Nat. Commun. **9**:3516.

Wierzbicki, A.T., Blevins, T., and Swiezewski, S. (2021). Long noncoding RNAs in plants. Annu. Rev. Plant Biol. **72**:245–271.

Xing, H.L., Dong, L., Wang, Z.P., Zhang, H.Y., Han, C.Y., Liu, B., Wang, X.C., and Chen, Q.J. (2014). A CRISPR/Cas9 toolkit for multiplex genome editing in plants. BMC Plant Biol. **14**:327.

Xu, S., Dong, Q., Deng, M., Lin, D., Xiao, J., Cheng, P., Xing, L., Niu, Y., Gao, C., Zhang, W., et al. (2021). The vernalization-induced long non-coding RNA VAS functions with the transcription factor TaRF2b to promote TaVRN1 expression for flowering in hexaploid wheat. Mol. Plant **14**:1525–1538.

Zhang, L., Chia, J.M., Kumari, S., Stein, J.C., Liu, Z., Narechania, A., Maher, C.A., Guill, K., McMullen, M.D., and Ware, D. (2009). A genome-wide characterization of microRNA genes in maize. PLoS Genet. **5**, e1000716.

Zhang, Y., Pitchiaya, S., Cieślik, M., Niknafs, Y.S., Tien, J.C.Y., Hosono, Y., Iyer, M.K., Yazdani, S., Subramaniam, S., Shukla, S.K., et al. (2018). Analysis of the androgen receptor-regulated lncRNA landscape identifies a role for ARLNC1 in prostate cancer progression. Nat. Genet. **50**:814–824.

Zhang, Y.C., Liao, J.Y., Li, Z.Y., Yu, Y., Zhang, J.P., Li, Q.F., Qu, L.H., Shu, W.S., and Chen, Y.Q. (2014). Genome-wide screening and functional analysis identify a large number of long noncoding RNAs involved in the sexual reproduction of rice. Genome Biol. **15**:512.

Zhao, X., Li, J., Lian, B., Gu, H., Li, Y., and Qi, Y. (2018). Global identification of Arabidopsis lncRNAs reveals the regulation of MAF4 by a natural antisense RNA. Nat. Commun. **9**:5056.

Zhu, H., Hu, F., Wang, R., Zhou, X., Sze, S.H., Liou, L.W., Barefoot, A., Dickman, M., and Zhang, X. (2011). Arabidopsis Argonaute10 specifically sequesters miR166/165 to regulate shoot apical meristem development. Cell **145**:242–256.